Quantum control and quantum speed limits in supersymmetric potentials

PAPER • OPEN ACCESS

Quantum control and quantum speed limits in supersymmetric potentials

To cite this article: C Campbell *et al* 2022 *New J. Phys.* **24** 095001

New Journal of Physics
The open access journal at the forefront of physics

Deutsche Physikalische Gesellschaft DPG
IOP Institute of Physics

Published in partnership with: Deutsche Physikalische Gesellschaft and the Institute of Physics

OPEN ACCESS

RECEIVED
27 June 2022

REVISED
26 July 2022

ACCEPTED FOR PUBLICATION
15 August 2022

PUBLISHED
6 September 2022

PAPER

Quantum control and quantum speed limits in supersymmetric potentials

C Campbell[1,*], J Li[2], Th Busch[1] and T Fogarty[1]

[1] Quantum Systems Unit, Okinawa Institute of Science and Technology Graduate University, Onna, Okinawa 904-0495, Japan
[2] Department of Physics, University College Cork, Cork, Ireland
[*] Author to whom any correspondence should be addressed.

E-mail: christopher.campbell@oist.jp

Keywords: supersymmetry, quantum gases, shortcuts to adiabaticity, quantum speed limits

Abstract

Supersymmetry allows one to build a hierarchy of Hamiltonians that share the same spectral properties and which are pairwise connected through common super-potentials. The iso-spectral properties of these Hamiltonians imply that the dynamics and therefore control of different eigenstates are connected through supersymmetric intertwining relations. In this work we explore how this enables one to study general dynamics, shortcuts to adiabaticity and quantum speed limits for distinct states of different supersymmetric partner potentials by using the infinite box as an example.

1. Introduction

Ultracold atoms have become a leading contender for applications in future quantum technologies due to the possibility to control nearly all their degrees of freedom with high fidelities [1, 2]. For their center-of-mass degree of freedom this is due to immense technical advancements in recent years where almost arbitrary trapping potentials can be designed with spatial light modulators, while optical tweezer arrays allow for the precise control of single particles and the ability to build many-body systems one particle at a time [3–5]. One of the few bottlenecks that remains is to design dynamical protocols that allow for minimal operation times of quantum devices, while preventing non-equilibrium excitations from destroying the fragile quantum states and therefore resulting in low fidelity processes. Bounds on this minimal time are commonly known as quantum speed limits (QSLs) [6], and are often based on time-energy uncertainty relations. They have been thoroughly researched in recent years and also been extended to mixed states, driven dynamics and open systems [7–10].

One class of technique that allows people to develop protocols that operate as close to the QSL as possible while retaining high fidelities are shortcuts to adiabaticity (STAs). These ensure robust adiabatic-like dynamics of quantum states on non-adiabatic timescales and a plethora of techniques to design them are known (see [11] for a recent review). Among them are, for example, inverse engineering of optimal time-dependent parameters of a Hamiltonian from the knowledge of the desired adiabatic dynamics of the system [12, 13], or adding auxiliary fields designed to minimize unwanted excitations during driven dynamics [14]. An important subset of STAs deal with scale-invariant dynamics [15] which allow to generalize control parameters for different potentials, a well known example being the modulation of the trap frequency of the harmonic oscillator. In fact, while methods in this subset are usually restricted to single-particle systems, in the specific case of the harmonic oscillator they can also be applied to the many-body system of a unitary Fermi gas [16] and the self-similar dynamics of the total density can also allow for the experimental extraction of the QSL [17, 18]. The speedup that can be gained from STAs is considered to be of importance for creating quantum devices that suffer from decoherence, but they have recently also found important applications in the area of quantum thermodynamic devices and in particular quantum engines [19–24].

In this work we explore the dynamics and the use of STAs for the specific situation of a family of Hamiltonians which are related via consecutive supersymmetric transformations [25–28]. A unique property of these Hamiltonians is that their energy spectra are degenerate [29], however the eigenstates of each Hamiltonian are unique. Moreover, the degenerate states are also directly connected via supersymmetric transformations, which can be used to describe their non-equilibrium dynamics [30]. Supersymmetric Hamiltonians therefore offer an enticing platform with which to explore how dynamical control is related between systems with shared spectral properties, while the supersymmetric algebra is also amenable to exact analytical calculations. Specifically, in this work we will focus on the dynamics of both isospectral states and the individual ground states of each potential, the latter of which have different energies. This will allow us to gain insight into the effects on the QSL stemming from the energy for different states in the spectrum vs the ones coming from the distance between the initial and the final state in Hilbert space. In particular we consider the example of an expanding infinite box and the related higher order supersymmetric partner Hamiltonians [30, 31] and show analytically that the knowledge of the shortcut for the initial Hamiltonian translates through the superpotential to all higher order ones. This then allows to efficiently construct the control parameters for any Hamiltonian in this connected supersymmetric hierarchy. This also has consequences for the energetic cost of performing the STA and the associated QSL of maintaining the high fidelity dynamics, and which we show can be related through supersymmetric transformations. Our work therefore shows the versatility of supersymmetric Hamiltonians for use in quantum control protocols and their potential for investigating QSLs in connected systems.

2. Scale invariant dynamics

Throughout this work we will consider a family of one-dimensional Hamiltonians for a particle in different potentials, which are all parametrized by a length $L(t)$ that can be smoothly changed over a total period τ. The time dependent Hamiltonians are labeled by a positive integer α and given by

$$H^{(\alpha)}(x,t) = -\frac{\hbar^2}{2m}\frac{\partial^2}{\partial x^2} + V^{(\alpha)}(x,t), \tag{1}$$

and as our starting point ($\alpha = 1$) we choose an infinite box potential given by

$$V^{(1)}(x,t) = \begin{cases} \infty, & \text{if } |x| > \dfrac{L(t)}{2}, \\ 0, & \text{if } |x| < \dfrac{L(t)}{2}, \end{cases} \tag{2}$$

with the well known instantaneous eigenstates $\psi_n^{(1)}(x,t) = \sqrt{\frac{2}{L(t)}}\,\sin(n\pi\left(\frac{x}{L(t)} + \frac{1}{2}\right))$ and energies $\mathcal{E}_n^{(1)}(t) = \frac{n^2\pi^2\hbar^2}{2mL(t)^2}$. Using the box as the original potential is motivated by the fact that the supersymmetric partner potentials and their eigenstates are well known, which also allows us to describe the dynamics of these systems to a large degree analytically [31].

In this case $L(t)$ gives the width of the box and we parameterize it as $L(t) = \gamma(t)L_\mathrm{i}$, where $\gamma(t)$ is a time dependent scaling factor, and we choose it to be a *smoother step function* [32]

$$\gamma(t) = \frac{L(t)}{L_\mathrm{i}} = 1 + \left[\frac{L_\mathrm{f}}{L_\mathrm{i}} - 1\right]\left(\frac{t}{\tau}\right)^3\left[10 + 3\frac{t}{\tau}\left(2\frac{t}{\tau} - 5\right)\right], \tag{3}$$

where L_i is the length at $t = 0$ and L_f at the final time τ. This ramp for the infinite box potential has previously been studied [13] and in the following we will explore the dynamics induced by this ramp for a hierarchy of Hamiltonians which are related to $H^{(1)}$ via a supersymmetric algebra and therefore have an almost identical energy spectrum.

In its simplest form, the algebra of supersymmetric quantum mechanics looks to create pairs of Hamiltonians using a set of unique adjoint operators, namely $H^{(\alpha)} = A^{(\alpha)\dagger}A^{(\alpha)} + \mathcal{E}_1^{(\alpha)}$ and $H^{(\alpha+1)} = A^{(\alpha)}A^{(\alpha)\dagger} + \mathcal{E}_1^{(\alpha)}$, where $\alpha \geqslant 1$ accounts for the order of the supersymmetric transformation and $\mathcal{E}_1^{(\alpha)}$ is the respective groundstate energy of potential of order α [25, 26, 33]. These operators act as creation and annihilation operators and can be explicitly written as

$$A^{(\alpha)} = \frac{\hbar}{\sqrt{2m}}\frac{\mathrm{d}}{\mathrm{d}x} + \mathcal{W}^{(\alpha)}(x), \tag{4}$$

$$A^{(\alpha)\dagger} = -\frac{\hbar}{\sqrt{2m}}\frac{\mathrm{d}}{\mathrm{d}x} + \mathcal{W}^{(\alpha)}(x), \tag{5}$$

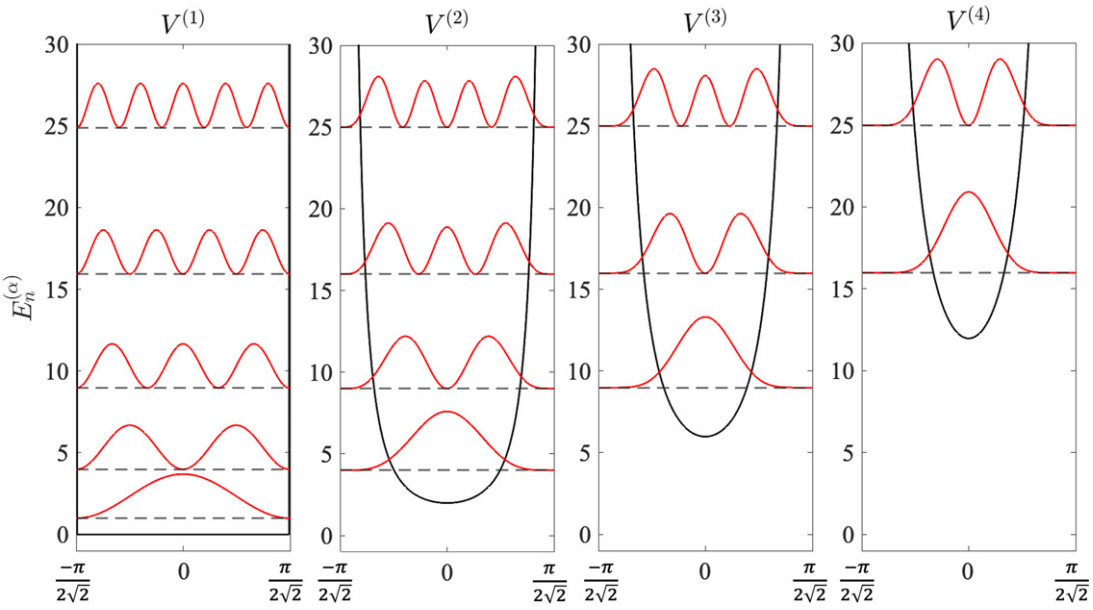

Figure 1. Eigenspectrum (dashed lines) and eigenfunctions (red lines) of the infinite box potential $V^{(1)}$ and the three next higher order supersymmetric partner potentials (full lines). For the purpose of this work we use $L_i = \frac{\pi}{\sqrt{2}}$. One can see that all eigenspectra are degenerate, however each subsequent potential removes the lowest lying energy of the previous one.

where $\mathcal{W}^{(\alpha)}(x)$ is the so-called superpotential. This allows us to write the partner potentials of Hamiltonians $H^{(\alpha)}$ and $H^{(\alpha+1)}$ as

$$V^{(\alpha),(\alpha+1)} = \left[\mathcal{W}^{(\alpha)}(x,t)\right]^2 \mp \frac{\hbar}{\sqrt{2m}}\frac{\mathrm{d}}{\mathrm{d}x}\left[\mathcal{W}^{(\alpha)}(x,t)\right], \tag{6}$$

with the sign between the two terms being negative (positive) for $H^{(\alpha)}$ ($H^{(\alpha+1)}$). Since in our case $V^{(1)}$ is the infinite box potential (see equation (2)), one can find an explicit expression for the superpotential $\mathcal{W}^{(1)}$ by applying the annihilation operator $A^{(1)}$ to the ground state of the potential, which through algebraic rearranging is written as

$$\begin{aligned}\mathcal{W}^{(1)}(x,t) &= -\frac{\hbar}{\sqrt{2m}}\partial_x \ln(\psi_1^{(1)}(x,t)) \\ &= \frac{\hbar\pi}{\sqrt{2m}L(t)}\tan\left(\frac{\pi x}{L(t)}\right),\end{aligned} \tag{7}$$

and consequently the form of the first partner potential as

$$V^{(2)}(x,t) = \frac{\hbar^2\pi^2}{2mL(t)^2}\left(\sec^2\left(\frac{x\pi}{L(t)}\right) + \tan^2\left(\frac{\pi x}{L(t)}\right)\right), \tag{8}$$

with its ground state [30, 31]

$$\psi_1^{(2)} = \sqrt{\frac{2}{3L(t)}}\cos\left(\frac{\pi x}{L(t)}\right)^2. \tag{9}$$

This process can be repeated to obtain higher order supersymmetric Hamiltonians and one can find a general form for the superpotential as

$$\mathcal{W}^{(\alpha)}(x,t) = \frac{\alpha\hbar\pi}{\sqrt{2m}L(t)}\tan\left(\frac{\pi x}{L(t)}\right). \tag{10}$$

One of the most important features of such a supersymmetric hierarchy of Hamiltonians is that their eigenspectra are identical, however each higher order one removes the previously lowest lying ground state, i.e. $\mathcal{E}_n^{(\alpha+1)} = \mathcal{E}_{n+1}^{(\alpha)}$ (see figure 1). The spectrum of any supersymmetric partner Hamiltonian of the infinite square well is therefore given by

$$\mathcal{E}_n^{(\alpha)}(t) = \frac{(n+\alpha-1)^2\pi^2\hbar^2}{2mL(t)^2}, \tag{11}$$

and one can see the change in the length $L(t)$ effects all spectra in a predictable and straightforward way irrespective of the order of the partner potentials. This allows one to explore the dynamics of different states

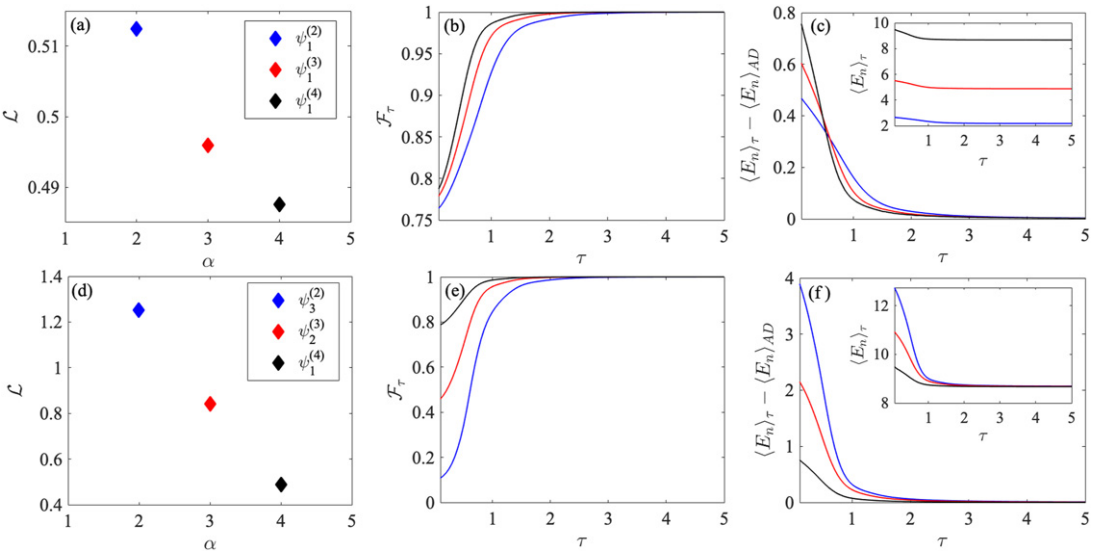

Figure 2. (a) and (d) Bures angle, (b) and (e) fidelity and (c) and (f) time averaged excess energy as a function of the ramp time τ. The insets in panels (c) and (f) show the time averaged energy and we take $L_\mathrm{i} = \frac{\pi}{\sqrt{2}}$ throughout. The states are taken from the first three partner Hamiltonians of the infinite box with (a)–(c) all of the ground state wavefunctions and (d)–(f) wavefunctions with an instantaneous energy of $\mathcal{E}_n^{(\alpha)}(t) = \frac{16\pi^2\hbar^2}{2mL(t)^2}$. Note that the y-axis scales differ significantly between the top and bottom rows, highlighting the differences between the two sets of states.

in the presence of the same spectrum and therefore cleanly separate the influences of the spectrum from the effects stemming from the distance between the initial and final state in Hilbert space. The latter can be quantified by the Bures angle

$$\mathcal{L}^{(\alpha)} = \arccos\left(\left|\left\langle\psi_n^{(\alpha)}(x,0)|\psi_n^{(\alpha)}(x,\tau)\right\rangle\right|\right). \tag{12}$$

which describes the geometric distance between the initial state at time $t = 0$ and the target state at $t = \tau$ [34].

In the following we will study two specific settings in which we double the lengthscale of the initial potential L_i, such that at the end of the ramp $L_\mathrm{f} = L(\tau) = 2L_\mathrm{i}$. In the first case we look at the respective groundstates $\psi_1^{(\alpha)}$ of the different supersymmetric partner potentials $V^{(2)}$, $V^{(3)}$ and $V^{(4)}$, for which the Bures angle is shown in figure 2(a). The Bures angle highlights that the geometric distance that each groundstate needs to travel through Hilbert space is roughly equivalent, whereas the change in energy between the initial and final eigenstates, $\mathcal{E}_1^{(\alpha)}(\tau) - \mathcal{E}_1^{(\alpha)}(0) = \frac{\alpha^2\pi^2\hbar^2}{2m}\left(\frac{1}{L_\mathrm{f}^2} - \frac{1}{L_\mathrm{i}^2}\right)$ is dependent on the order of the potential α and naively suggests differences in their dynamics.

Therefore, the second case we consider is a set of eigenstates that have the same energy within the isospectral setting of different supersymmetric Hamiltonians. In particular we use the states $|\psi_3^{(2)}\rangle$, $|\psi_2^{(3)}\rangle$ and $|\psi_1^{(4)}\rangle$ as the initial state, which all have the same instantaneous energy $\mathcal{E}_n^{(\alpha)}(t) = \frac{16\pi^2\hbar^2}{2mL(t)^2}$. The energy change during an adiabatic ramp is therefore identical for all of them, however, the corresponding Bures angles are quite different (see figure 2(d)), with the geometric distance growing for increasing quantum number n.

Next we explore the finite time dynamics of each initial eigenstate $\psi_n^{(\alpha)}(x,0)$ during the expansion process using the ramp given in equation (3), which leads to a state at the end of the unitary dynamics that is given by $|\Psi_n^{(\alpha)}(x,\tau)\rangle = \mathcal{T}\,\mathrm{e}^{-\frac{\mathrm{i}}{\hbar}\int_0^\tau H^{(\alpha)}(x,t')\mathrm{d}t'}|\psi_n^{(\alpha)}(x,0)\rangle$, where $\mathcal{T}$ is the time-ordering operator. The adiabaticity of the driven dynamics can be quantified using the single particle fidelity $\mathcal{F}(\tau) = |\langle\psi_n^{(\alpha)}(x,\tau)|\Psi_n^{(\alpha)}(x,\tau)\rangle|^2$, which compares the state at the end of the unitary dynamics $\Psi_n^{(\alpha)}(x,\tau)$ with the instantaneous eigenstate $\psi_n^{(\alpha)}(x,\tau)$. If the length scale of the potential is changed slowly, $\tau \to \infty$, the fidelity is one as $\Psi_n^{(\alpha)}(x,\tau) = \psi_n^{(\alpha)}(x,\tau)$ and the dynamics is considered adiabatic. However, for faster ramps the system can be driven far from equilibrium, which results in a reduced fidelity $\mathcal{F}(\tau) < 1$.

The fidelity for the two sets of initial states we consider is shown as a function of τ in figures 2(b) and (e). As expected, in both cases the fidelity is unity for ramp times $\tau \geqslant 4$, while it decreases for faster ramps. However, it is clear that at these short ramp times the fidelity of the two cases is quite different. When considering the groundstates of each potential (panel (b)) the differences in the fidelity are small, and even for very short times the fidelity is still above 70%. The reason for this rather high value can be found in the Bures angle, as despite the initial and the target state being different, they are still geometrically rather close

in Hilbert space and the system can therefore be driven rather fast. In fact, the fidelity and the Bures angle are similar for all three partner potentials shown here, indicating a rather similar dynamics. On the other hand, the results for the isospectral initial states possess quite different fidelities in a range from 80% to 10%, which is in agreement with the Bures angle indicating that these states have very different geometric distances.

This behaviour is also evident in the amount of non-equilibrium excitations that are created during the trap ramp, which can be quantified using the time average energy

$$\langle E_n\rangle_\tau = \frac{1}{\tau}\int_0^\tau \mathrm{d}t \langle \Psi_n^{(\alpha)}(t)|H^{(\alpha)}(t)|\Psi_n^{(\alpha)}(t)\rangle. \tag{13}$$

For an adiabatic process, where the evolving state $\Psi_n^{(\alpha)}(t)$ is always an eigenstate of $H^{(\alpha)}(t)$, this average energy is equal to the adiabatic energy $\langle E_n\rangle_{\mathrm{AD}} = \frac{1}{\tau}\int_0^\tau \mathrm{d}t\, \mathcal{E}_n^{(\alpha)}(t)$, where the $\mathcal{E}_n^{(\alpha)}(t)$ are the instantaneous energies given in equation (11). In figures 2(c) and (f) we plot the energy differences $\langle E_n\rangle_\tau - \langle E_n\rangle_{\mathrm{AD}}$, which again vanish for large τ, while being finite for faster ramps. Comparing the two cases we consider, the excess energies for the groundstate dynamics only show minor differences, while for the isospectral initial states the non-equilibrium excitations increase the further the states are apart in Hilbert space. This reflects the results for the fidelity, suggesting that the instantaneous energy of each individual state does not play a major role in reaching a high fidelity target state.

One can further explore the above dynamics by relating the observed results to the QSL time, which bounds the minimum time to connect the two states $\psi_n(x,0)$ and $\psi_n(x,\tau)$. For our system it is given by [35]

$$\tau \geqslant \tau_{\mathrm{QSL}} \equiv \frac{\hbar}{2\langle E_n\rangle_\tau}[\sin(\mathcal{L})]^2, \tag{14}$$

and it is immediately clear that for the groundstates of the supersymmetric partner potentials the QSL time is only dependent on the average energy $\langle E_n\rangle_\tau$, as the Bures angle is effectively unchanged. On the contrary, for isospectral states the average energy for adiabatic ramps ($\tau\to\infty$) is fixed regardless of the chosen state, while the Bures angle decreases for increasing n. Again, the shared properties of supersymmetric Hamiltonians allow to easily compare the dynamical properties of states across the hierarchy of connected Hamiltonians, while adding further insights into controlled dynamics which will be discussed in the next section.

3. Shortcuts to adiabaticity and cost

The natural next step is to explore the precise control of the expansion dynamics to ensure perfect fidelity for all ramp times τ. For this task we employ STA, and while different methods can be applied to our problem [11], here we only focus on the technique of counterdiabatic driving. For this an auxiliary Hamiltonian is added to the single particle Hamiltonian in equation (1), $H_{\mathrm{STA}}^{(\alpha)}(t) = \mathrm{i}\hbar\hat{U}(t)^\dagger\partial_t\hat{U}(t) = H^{(\alpha)}(t) + H_{\mathrm{CD}}^{(\alpha)}(t)$ which effectively nullifies nonadiabatic excitations and ensures that the driven state always follows the instantaneous eigenstate $\Psi_n^{(\alpha)}(x,t) = \mathrm{e}^{-\mathrm{i}\int^t \mathcal{E}_n(t')\mathrm{d}t'}\psi_n^{(\alpha)}(x,t)$, realizing adiabatic dynamics for any value of τ. Using the time evolution operator $\hat{U}(t,t'=0) = |\Psi_n^{(\alpha)}(x,t)\rangle\langle\psi_n^{(\alpha)}(x,0)|$ the counterdiabatic driving term is given by [36–38]

$$H_{\mathrm{CD},n}^{(\alpha)}(t) = \mathrm{i}\hbar\big|\partial_t\psi_n^{(\alpha)}(t)\big\rangle\big\langle\psi_n^{(\alpha)}(t)\big|, \tag{15}$$

and since the eigenstates of the full hierarchy of the supersymmetric Hamiltonians related to the infinite box can be written in terms of Chebyshev polynomials of the second kind [31], it can be exactly evaluated. However, these general expressions can become unwieldly for excited states in higher order Hamiltonians very quickly, and we therefore restrict ourselves here to an illustrative example for the groundstate and first excited state of $H^{(\alpha)}$, which allows us to contrast both groundstate and isospectral STAs. These are given by

$$\psi_1^{(\alpha)} = \frac{1}{\sqrt{L(t)}}\left[\frac{\sqrt{\pi}\Gamma(\alpha+1)}{\Gamma\left(\alpha+\frac{1}{2}\right)}\right]^{\frac{1}{2}}\cos\left(\frac{x\pi}{L(t)}\right)^\alpha, \tag{16}$$

$$\partial_t\psi_1^{(\alpha)} = \psi_1^{(\alpha)}\left[-\frac{1}{2} + \frac{\pi x\alpha}{L(t)}\tan\left(\frac{\pi x}{L(t)}\right)\right]\frac{\dot{L}(t)}{L(t)}, \tag{17}$$

and

$$\psi_2^{(\alpha)} = \frac{1}{\sqrt{L(t)}}\left[\frac{2\sqrt{\pi}\Gamma(\alpha+2)}{\Gamma\left(\alpha+\frac{1}{2}\right)}\right]^{\frac{1}{2}}\sin\left(\frac{x\pi}{L(t)}\right)\cos\left(\frac{x\pi}{L(t)}\right)^\alpha, \tag{18}$$

$$\partial_t \psi_2^{(\alpha)} = \psi_2^{(\alpha)} \left[-\frac{1}{2} - \frac{\pi x}{L(t)} \tan^{-1}\left(\frac{x\pi}{L}\right) + \frac{x\pi\alpha}{L(t)} \tan\left(\frac{x\pi}{L}\right) \right] \frac{\dot{L}(t)}{L(t)}, \tag{19}$$

and when inserting them into equation (15) one can immediately note that the CD term in both cases is proportional to $\dot{L}(t)/L(t)$ for all α, consistent with known STAs for the infinite box potential [15, 39].

Furthermore, by recalling the intertwining properties of supersymmetric Hamiltonians, $A^{(\alpha)}H^{(\alpha)} = H^{(\alpha+1)}A^{(\alpha)}$ and $H^{(\alpha)}A^{(\alpha)\dagger} = A^{(\alpha)\dagger}H^{(\alpha+1)}$ [40], we can show a similar relation for the counterdiabatic term [28]. The above intertwining relations between $H^{(\alpha)}$ and $H^{(\alpha+1)}$ allow one to transform two degenerate sets of stationary states through

$$|\psi_{n-1}^{(\alpha+1)}\rangle = \frac{A^{(\alpha)}}{\sqrt{\Delta\mathcal{E}_n^{(\alpha)}}} |\psi_n^{(\alpha)}\rangle, \tag{20}$$

$$|\psi_n^{(\alpha)}\rangle = \frac{A^{(\alpha)\dagger}}{\sqrt{\Delta\mathcal{E}_n^{(\alpha)}}} |\psi_{n-1}^{(\alpha+1)}\rangle, \tag{21}$$

where $\Delta\mathcal{E}_n^{(\alpha)} = \mathcal{E}_n^{(\alpha)} - \mathcal{E}_1^{(\alpha)}$ is the difference in energy between the nth state and the ground state of $H^{(\alpha)}$. This then directly allows one to write an expression for the intertwining relation of the counterdiabatic term as

$$\begin{aligned} H_{\mathrm{CD},n}^{(\alpha+1)} &= \mathrm{i}\hbar\partial_t \left|\psi_n^{(\alpha+1)}\right\rangle\left\langle\psi_n^{(\alpha+1)}\right| \\ &= \frac{\mathrm{i}\hbar}{\Delta\mathcal{E}_{n+1}^{(\alpha)}} \partial_t \left(A^{(\alpha)}\left|\psi_{n+1}^{(\alpha)}\right\rangle\right)\left\langle\psi_{n+1}^{(\alpha)}\right| A^{(\alpha)\dagger} \\ &= \frac{1}{\Delta\mathcal{E}_{n+1}^{(\alpha)}} A^{(\alpha)} H_{\mathrm{CD},n+1}^{(\alpha)} A^{(\alpha)\dagger} + \frac{\mathrm{i}\hbar}{\Delta\mathcal{E}_{n+1}^{(\alpha)}} (\partial_t A^{(\alpha)})\left|\psi_{n+1}^{(\alpha)}\right\rangle\left\langle\psi_{n+1}^{(\alpha)}\right| A^{(\alpha)\dagger}, \end{aligned} \tag{22}$$

where $H_{\mathrm{CD},n+1}^{(\alpha)} = \mathrm{i}\hbar|\partial_t\psi_{n+1}^{(\alpha)}\rangle\langle\psi_{n+1}^{(\alpha)}|$ is the counterdiabatic Hamiltonian for the state $|\psi_{n+1}^{(\alpha)}\rangle$, which has the same instantaneous energy as $|\psi_n^{(\alpha+1)}\rangle$, and the second term arises due to the time-dependence of the supersymmetric operator $A^{(\alpha)}$. While this expression for the intertwining relations of the counterdiabatic Hamiltonian is not as simple as for the system Hamiltonian alone, it shows that the counterdiabatic term for the next higher supersymmetric Hamiltonian can be constructed with only knowledge of the lower lying Hamiltonian and its eigenstates [28].

Let us next look at the relationship between the QSL and the energetic cost of the counterdiabatic term [35]. In our case this cost is defined as the energy required to achieve adiabatic dynamics for a specific expansion stroke and a common way to quantify this is given by the trace norm of the counterdiabatic driving term $C_n^{(\alpha)} = \int_0^\tau \mathrm{d}t \|H_{\mathrm{CD},n}^{(\alpha)}\|_{\mathrm{tr}}$ [41] where the integrand can be written in terms of the instantaneous eigenstates as

$$\partial_t C_n^{(\alpha)} = \sqrt{\langle\partial_t\psi_n^{(\alpha)}|\partial_t\psi_n^{(\alpha)}\rangle}. \tag{23}$$

Taking the above expressions, it is straightforward to find the cost of implementing the STA for the ground state of any supersymmetric Hamiltonian $H^{(\alpha)}$ as

$$\partial_t C_1^{(\alpha)} = \frac{\dot{L}(t)}{L(t)} \left[-\frac{1}{4} + \int_{-L(t)/2}^{L(t)/2} \psi_1^{(\alpha)}\psi_1^{(\alpha)*} \left(\frac{\pi x\alpha}{L(t)} \tan\left(\frac{x\pi}{L(t)}\right)\right)^2 \mathrm{d}x \right]^{\frac{1}{2}}, \tag{24}$$

where it is worth noting that the leading term is independent of α, while the integral is order dependent. To compare isospectral states in different order Hamiltonians the costs can be shown to be again related by supersymmetric transformations. Using the explicit expressions given above for the ground and first excited state of adjacent supersymmetric Hamiltonians we get

$$\partial_t C_2^{(\alpha-1)} = \frac{\dot{L}(t)}{L(t)} \left[-\frac{1}{4} + (2\alpha-1) \int_{-L(t)/2}^{L(t)/2} \psi_1^{(\alpha)*}\psi_1^{(\alpha)} \left(\frac{x\pi}{L(t)}\right)^2 \left(1 + (1-\alpha)\tan\left(\frac{x\pi}{L(t)}\right)^2\right)^2 \mathrm{d}x \right]^{\frac{1}{2}}, \tag{25}$$

with the leading term still independent of α. Such a relation can be found for any set of eigenstates in the supersymmetric hierarchy which possess the same instantaneous energy.

In figure 3 we show the time average cost $\langle\partial_t C_n^{(\alpha)}\rangle_\tau = \frac{1}{\tau}\int_0^\tau \partial_t C_n^{(\alpha)}\,\mathrm{d}t$ as a function of the ramp time τ for the groundstates (panel (a)). One can see that the cost is diverging for short times ($\tau \to 0$), where more energy is required to keep the system adiabatic. Interestingly, despite the different states having different energies and also a different energy gap to the next higher state in the spectrum,

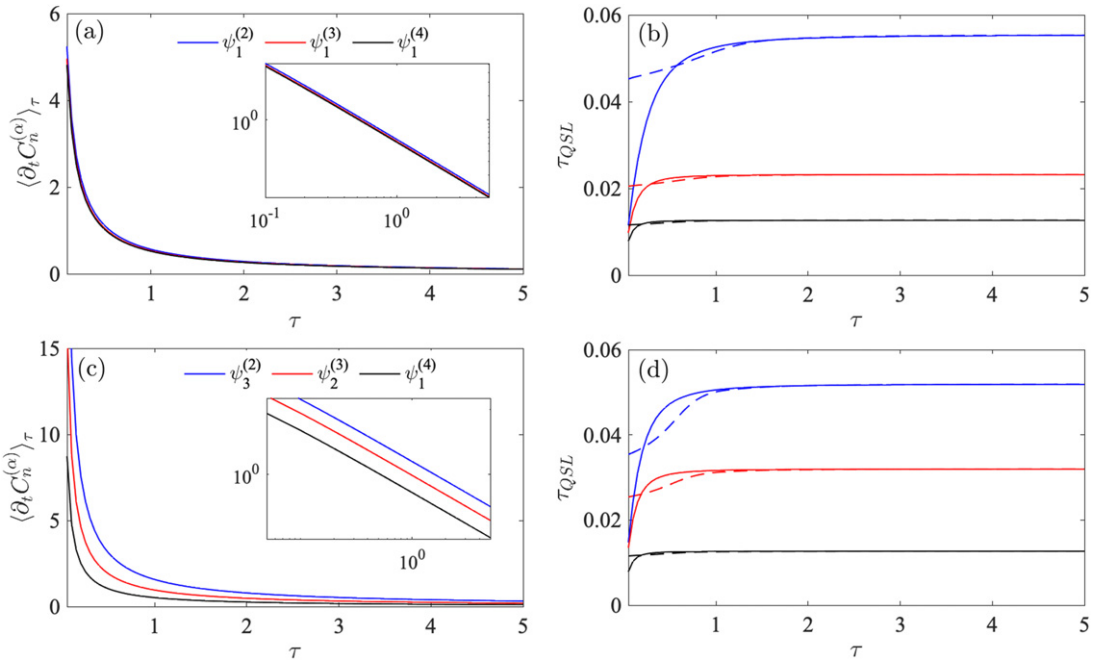

Figure 3. (a) and (c) Time averaged cost $\langle \partial_t C_n^{(\alpha)} \rangle_\tau = \frac{1}{\tau}\int_0^\tau \partial_t C_n^{(\alpha)}\, \mathrm{d}t$ (insets are in log–log scale) and (b) and (d) QSL time as a function of ramp duration τ. Panels (a) and (b) show results for the ground states of the first three partner Hamiltonians and panels (c) and (d) for the isospectral states. In panels (b) and (d) the dashed lines are the QSL times of the non-adiabatic dynamics equation (14), and solid lines are QSL times for the STA dynamics equation (26).

$\mathcal{E}_2^{(\alpha)} - \mathcal{E}_1^{(\alpha)} \neq \mathcal{E}_2^{(\alpha+1)} - \mathcal{E}_1^{(\alpha+1)}$, the cost for each groundstate is approximately equal (see inset for log–log scale) as the integral in equation (24) only varies weakly with α. This is vastly different for the isospectral case shown in panel (c). Here the mean cost increases for higher excited states, which is consistent with the results concerning the fidelity and energy for the non-adiabatic dynamics shown in figure 2. We can therefore conclude that states whose wavefunction possesses more nodes (which have a higher quantum number n) are less robust and require a larger energetic cost to remain adiabatic during a controlled expansion.

Finally, in figures 3(b) and (d) we show the QSL time for both the non-adiabatic (equation (14)) and the STA dynamics. For the latter it is given by [35]

$$\tau_{\mathrm{QSL}} = \frac{\hbar\tau[\sin(\mathcal{L}_\tau)]^2}{2\int_0^\tau \mathrm{d}t\sqrt{\mathcal{E}_n^2 + (\partial_t C)^2}}, \tag{26}$$

where the cost of the STA is now included in the denominator. For the groundstate comparison (panel (b)) the geometric distance and the STA costs vary only weakly between the states, but the instantaneous eigenvalues $\mathcal{E}_1^{(\alpha)}$ are quite different and are the main factor in the large differences in the QSL time. In comparison, the isospectral states have the same instantaneous energy $\mathcal{E}_n^{(\alpha)}$, however the distance and the cost are unique for each state, which results in the distinct QSL times. Furthermore, we can compare the QSL time for the STA with that of the non-adiabatic driving in equation (14). Obviously, at long times they converge as both dynamics become adiabatic, while at short times $\tau \to 0$ the STA can lower the QSL time to vanishing values. On the contrary, the non-adiabatic QSL time on these timescales is finite, as for $\tau = 0$ this simply describes a sudden quench of the trap potential, while the reduction in the QSL time is a consequence of the non-equilibrium excitations that allow the system to be driven faster from its initial state.

4. Conclusions

We have used the specific properties of supersymmetric partner potentials of the infinite box to explore the controlled dynamics through counterdiabatic driving. Supersymmetry provides a framework to explore STA protocols under different conditions and it allows one to compare and contrast different situations while constraining certain parameters. In fact, we have shown that eigenstates of different supersymmetric partner potentials share common properties, such as the Bures angle and eigenspectrum, therefore offering a convenient platform to investigate how these individually contribute to both non-equilibrium dynamics and

quantum control. The two sets of eigenstates that we considered in this work, namely the groundstates and a set of isospectral states of each partner potential, are unique to the hierarchy of supersymmetric Hamiltonians and possess distinct dynamics. Specifically, we have shown that both the non-equilibrium and STA dynamics of the groundstates are closely related as they share comparable geometric distances. On the contrary, the dynamics of isospectral states and the degree of control required by the STA, is strongly dependent on the specific state regardless of their energy. Moreover, these states are related through their shared superpotentials which allowed us to show that dynamical quantities, such as the counterdiabatic term and the cost for implementing it, transfer over seamlessly as a consequence of the intertwining properties, allowing one to build the control for the entire hierarchy of Hamiltonians from the knowledge of just one set of known eigenstates.

While we only consider the infinite box potential and its partner potentials in this work, we note that our analysis should qualitatively hold for scale invariant dynamics in other well known supersymmetric potentials [15, 33]. Promising extensions to this work could explore dynamically driving between partner Hamiltonians or transforming between isospectral states using time dependent operators $A^{(\alpha)}(t)$ which may be analogous to shortcuts performed by trap deformation [42]. Furthermore, recent experimental advances have shown that supersymmetric potentials can be created using holographic optical traps [43]. Their work also uses supersymmetric quantum mechanics to design a trapping potential that supports any desired energy spectrum up to some maximum eigenstate. For this they build the final potential by iteratively finding the super-potential for each energy level starting from the top down. This exact approach and the experimental setup would allow to create the hierarchy of supersymmetric partner potentials and the isospectral states that we consider in our work. Finally, since the dynamics in our system is scale invariant, the QSL time can be measured experimentally by measuring the width of the atomic density through time-of-flight measurements [17].

Acknowledgments

This work was supported by the Okinawa Institute of Science and Technology Graduate University. TF acknowledges support under JSPS KAKENHI-21K13856. The authors are also grateful for the Scientific Computing and Data Analysis (SCDA) section of the Research Support Division at OIST. JL acknowledges support from the Science Foundation Ireland Frontiers for the Future Research Grant 'Shortcut-Enhanced Quantum Thermodynamics' No. 19/FFP/6951.

Data availability statement

The data that support the findings of this study are openly available at the following URL/DOI: https://github.com/thfogarty/SUSY_STA.

ORCID iDs

C Campbell https://orcid.org/0000-0002-5051-0100
J Li https://orcid.org/0000-0002-7565-3933
Th Busch https://orcid.org/0000-0003-0535-2833
T Fogarty https://orcid.org/0000-0003-4940-5861

References

[1] Dumke R *et al* 2016 *J. Opt.* **18** 093001
[2] Amico L *et al* 2021 *AVS Quantum Sci.* **3** 039201
[3] Nogrette F, Labuhn H, Ravets S, Barredo D, Béguin L, Vernier A, Lahaye T and Browaeys A 2014 *Phys. Rev.* X **4** 021034
[4] Barredo D, Lienhard V, de Léséleuc S, Lahaye T and Browaeys A 2018 *Nature* **561** 79
[5] Gauthier G, Bell T A, Stilgoe A B, Baker M, Rubinsztein-Dunlop H and Neely T W 2021 Dynamic high-resolution optical trapping of ultracold atoms *Advances in Atomic, Molecular, and Optical Physics* vol 70 ed L F Dimauro, H Perrin and S F Yelin (New York: Academic) pp 1–101
[6] Mandelstam L and Tamm I 1945 *J. Phys.* **9** 249
[7] Deffner S and Campbell S 2017 *J. Phys. A: Math. Theor.* **50** 453001
[8] del Campo A, Egusquiza I L, Plenio M B and Huelga S F 2013 *Phys. Rev. Lett.* **110** 050403
[9] O'Connor E, Guarnieri G and Campbell S 2021 *Phys. Rev.* A **103** 022210
[10] Poggi P M, Campbell S and Deffner S 2021 *PRX Quantum* **2** 040349
[11] Guéry-Odelin D, Ruschhaupt A, Kiely A, Torrontegui E, Martínez-Garaot S and Muga J G 2019 *Rev. Mod. Phys.* **91** 045001

[12] del Campo A 2011 *Phys. Rev.* A **84** 031606
[13] del Campo A and Boshier M G 2012 *Sci. Rep.* **2** 648
[14] Berry M V 2009 *J. Phys. A: Math. Theor.* **42** 365303
[15] Deffner S, Jarzynski C and del Campo A 2014 *Phys. Rev.* X **4** 021013
[16] Diao P, Deng S, Li F, Yu S, Chenu A, del Campo A and Wu H 2018 *New J. Phys.* **20** 105004
[17] del Campo A 2021 *Phys. Rev. Lett.* **126** 180603
[18] García-Pintos L P, Nicholson S B, Green J R, del Campo A and Gorshkov A V 2022 *Phys. Rev.* X **12** 011038
[19] Abah O and Lutz E 2017 *Europhys. Lett.* **118** 40005
[20] Li J, Fogarty T, Campbell S, Chen X and Busch T 2018 *New J. Phys.* **20** 015005
[21] Keller T, Fogarty T, Li J and Busch T 2020 *Phys. Rev. Res.* **2** 033335
[22] Fogarty T and Busch T 2020 *Quantum Sci. Technol.* **6** 015003
[23] Hartmann A, Mukherjee V, Niedenzu W and Lechner W 2020 *Phys. Rev. Res.* **2** 023145
[24] Myers N M, Abah O and Deffner S 2022 *AVS Quantum Sci.* **4** 027101
[25] Sukumar C V 1985 *J. Phys. A: Math. Gen.* **18** L57–61
[26] Cooper F, Ginocchio J N and Wipf A 1989 *J. Phys. A: Math. Gen.* **22** 3707–16
[27] del Campo A, Boshier M G and Saxena A 2014 *Sci. Rep.* **4** 5274
[28] Zelaya K and Hussin V 2020 *J. Phys. A: Math. Theor.* **53** 165301
[29] Andrianov A A, Borisov N V and Ioffe M V 1984 *Phys. Lett.* A **105** 19–22
[30] Campbell C, Fogarty T and Busch T 2022 *Phys. Rev. Res.* **4** 033014
[31] Gutierrez K, León E, Belloni M and Robinett R W 2018 *Eur. J. Phys.* **39** 065404
[32] Perlin K 2002 Improving noise *Proc. 29th Annual Conf. Computer Graphics and Interactive Techniques SIGGRAPH '02* (New York: Association for Computing Machinery) pp 681–2
[33] Cooper F, Khare A and Sukhatme U 1995 *Phys. Rep.* **251** 267–385
[34] Hübner M 1992 *Phys. Lett.* A **163** 239–42
[35] Campbell S and Deffner S 2017 *Phys. Rev. Lett.* **118** 100601
[36] Demirplak M and Rice S A 2003 *J. Phys. Chem.* A **107** 9937–45
[37] Demirplak M and Rice S A 2005 *J. Phys. Chem.* B **109** 6838–44
[38] del Campo A 2013 *Phys. Rev. Lett.* **111** 100502
[39] Jarzynski C 2013 *Phys. Rev.* A **88** 040101
[40] Kuru Ş, Teğmen A and Verçin A 2001 *J. Math. Phys.* **42** 3344–60
[41] Zheng Y, Campbell S, De Chiara G and Poletti D 2016 *Phys. Rev.* A **94** 042132
[42] Martínez-Garaot S, Palmero M, Muga J G and Guéry-Odelin D 2016 *Phys. Rev.* A **94** 063418
[43] Cassettari D, Mussardo G and Trombettoni A 2022 arXiv:2202.03446